Vortex-model-based Multi-objective Optimization of Winglets for Wind Turbines using Machine Learning

Leenders, Nick; Yu, Wei; Gaunaa, Mac; Caboni, Marco; Ferreira, Carlos Simão

DOI
10.1088/1742-6596/2265/3/032056

Publication date
2022

Document Version
Final published version

Published in
Journal of Physics: Conference Series

Vortex-model-based Multi-objective Optimization of Winglets for Wind Turbines using Machine Learning

Vortex-model-based Multi-objective Optimization of Winglets for Wind Turbines using Machine Learning

Nick Leenders[1,2], Wei Yu[1], Mac Gaunaa[2], Marco Caboni[3] and Carlos Simão Ferreira[1]

[1] Delft University of Technology, Kluyverweg 1, Delft, The Netherlands
[2] DTU Wind Energy, Risø Campus, Frederiksborgvej 399, Roskilde, Denmark
[3] TNO Petten, Westerduinweg 3, Petten, The Netherlands

E-mail: nickleenders@me.com

Abstract. Different Design Driving Load constraints (DDLs), are explored in this work to determine under which constraints and conditions a winglet can have an added value to the wind turbine blade design. Multi-objective Bayesian optimization is used to maximize the rotor's power production while minimizing the flapwise DDLs. Surrogate models, created using machine learning techniques such as Gaussian Processes and Bayesian Neural Networks, are used in combination with an acquisition function, to determine what designs should be evaluated by the lifting line model AWSM, with the goal to obtain designs that lie on the Pareto front of two or more objectives. The recent Bayesian Neural Networks as surrogate model were able to find the Pareto-front most effectively in this work. Furthermore, the results show that different DDL constraints led to different winglet designs, with noticeable differences between upwind and downwind winglet designs. Winglet designs were found to be able to increase power without increasing the thrust, root flapwise bending moment and flapwise bending moment at radial locations on the blade. A noticeable increase in power was found when introducing sweep to the winglet design.

1. Introduction

Rotors of wind turbines are increasing in size to reduce the Cost of Energy (CoE), by increasing the wind turbine's Annual Energy Production. By improving wind turbine blades using winglets, the energy yield can be increased. Although winglets are commonly used in modern airplane designs for jet aircraft or gliders, they are mostly absent on blade designs found in industry.
A winglet displaces the blade's trailing vortex and changes the induced velocities at the blade, which could increase the overall power production of the rotor. Ultimately, this changes the blade's load distribution, which could also increase unwanted flapwise loads on the blade. Whether a winglet can be beneficial to the blade design is highly dependent on the set constraints, as different constraints can result in different rotor designs as shown by Loenbaek [1].
This work will therefore investigate under which constraints the design of a wind turbine can actually benefit from a winglet, by minimizing the flapwise loads from the winglet while maximizing the power. For airplanes, winglets are usually pointing upwards due to ground clearance; however, for wind turbines, winglets pointing in the downwind or upwind direction are both viable options. Gaunnaa et al. [2] showed analytically in an axisymmetric setting that a downwind winglet serves to increase the power production contribution from the main part

of the blade. The downwind winglet itself has a negative contribution to the power production. However, for an upwind winglet it is the opposite, with a positive power contribution from the upwind winglet itself, and a lower power production from the blade. For the non-rotating case of an airplane winglet, Eppler [3] used a method to investigate the effect of the assumption of a rigid wake and found that a wing experiences induced lift forces, due to the velocities that lifting vortices induce on themselves. It was found that upwards pointing winglets let to positive induced lift and downwards pointing winglets to negative induced lift.
Numerical analyses of winglets on wind turbine blades have been done as well. Johansen and Sorensen [4] used CFD to investigate up- and downwind winglets. They found downwind winglets indeed performed better overall, increasing power productions especially for lower wind speeds. Zahle et al. [5] conducted an optimization study for an upwind winglet where the out-of-plane bending moment at $\frac{r}{R} = 0.9$ was constrained. It was found that the shape leading to the most increase (2.6%) in power without an increase in bending moment was a tip extension with a winglet shape. Under the same constraints, a straight tip extension only achieved an increase in power of 0.76%, showing that a winglet is preferred over a straight tip extension under certain load constraints. It was also found in this study that it was beneficial to sweep the winglet downstream for power production. No explanation for this increase was found. Munk's stagger [6] theorem states that the induced drag of all wings with the same projected shape and same projected circulation on a plane perpendicular to the freestream is equal.
A multi-objective winglet optimization was done by Reddy et al. [7]. It was found that a winglet was able to increase a rotor's power coefficient with only a marginal increase in thrust and moment coefficient.
Aerodynamic analysis methods, which can provide an insight into the aerodynamic loads of wind turbine blades with winglets, have long-running times. Moreover, the use of different objectives can require many iterations of the aerodynamic analysis method. Surrogate-assisted modeling can hence reduce the number of iterations needed to reach an optimized design. Machine learning methods such as Bayesian Neural Networks [8] or Gaussian Processes in Bayesian Optimization [9] have recently shown promising results in surrogate-assisted optimization.

2. Methodology

For this optimization study, a fully automated workflow is required to efficiently search the design space. The winglet therefore needs to be parameterized. In this work, a fairly simple parameterization method is chosen which represents the winglet in an intuitive way. This may lead to more parameters to be optimized and restricts the shape of the winglet. As a winglet modifies the load distribution on the blade, the blade's loading is optimized as well. Instead of optimizing for twist and chord separately, the loading on the blade and winglet is optimized by defining the angles of attack each airfoil should operate at in 2D beforehand. The optimization will now be performed using a polar containing only this chosen angle of attack and corresponding lift, drag and moment coefficients, termed a dummy polar. After optimization of the chord distribution of the blade, the blade is now run with the actual polars, instead of the dummy polar to determine the angle of attack the blade is running at. Using the actual angle of attack with the real polars, the blade can now be re-twisted to obtain a twist distribution which makes sure the blade runs on the earlier defined angle of attack.
The winglet in this work is designed for the DTU 10MW RF blade [10].

2.1. Winglet definition

The winglet parameters optimized in this work are shown in table 1. Lower and upper limits are set as the result of a parameter study, where parameters inside these limits led to converging results in the majority of cases. The manufacturability of the winglet is not taken into account in this work. The translation of these parameters to a downwind winglet is shown in figure 1 and

Table 1. The domain of winglet parameters used for the optimization

Symbol	Parameter	Lower limit	Upper limit	Unit
ϕ	Cant	0	90	degrees
λ	Sweep	-55	55	degrees
h	Height	1	8	m
r_w	Radius	0.1	1.5	m
$c_{w,t}$	Tip chord	0.1	1.0	m
$c_{w,r}$	Root chord	0.3	3.0	m
$CP_{1,y}$	Control point 1 y	0	3	m
$CP_{2,y}$	Control point 2 y	0	3	m
$CP_{2,x}$	Control point 2 x	0.94	0.995	m
$CP_{3,y}$	Control point 3 y	0.1	3	m

2. An upwind winglet would be pointing in the negative x-direction. The rotational direction is shown by Ω and the line a lies on the xy-axis. The sweep angle refers to winglet's leading edge line and positive sweep is termed downstream sweep in this work, whereas negative sweep is termed upstream sweep. Not be confused with downwind or upwind winglet, where a downwind winglet points in the positive x-direction and a upwind winglet in the negative x-direction.
Downwind winglets on wind turbines have the issue of decreasing the tower clearance. For simplification, it is therefore assumed that whenever a downwind winglet is considered, a downwind rotor is used.
The diameter of the rotor is kept constant to the original diameter of the DTU 10MW RF in this work, as a diameter constraint is assumed, meaning the winglet replaces a part of the blade. The loading on a part of the blade is optimized as well. This is done by modifying the chord distribution with Bézier curves, where the location of the three control points is optimized, where all control points are able to move in y and one control point is able to move in x.

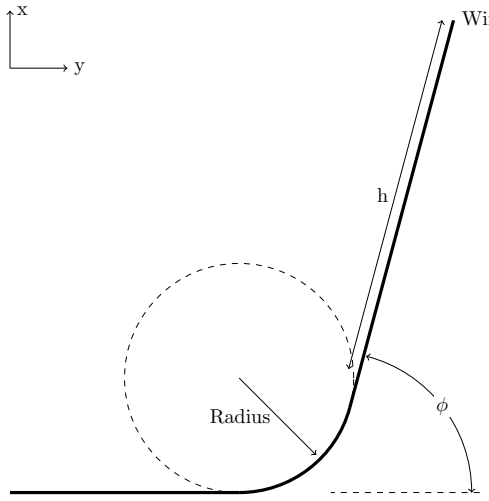

Figure 1. Two-dimensional view of a downwind winglet

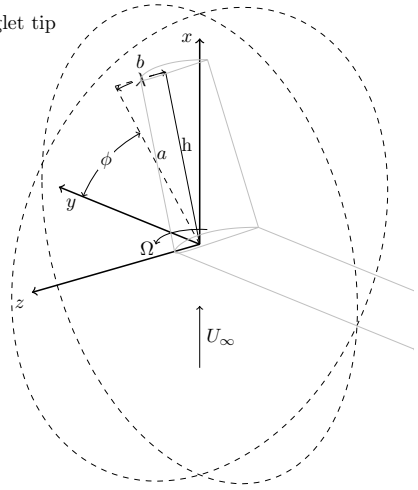

Figure 2. Definition of a winglet with parameter symbols shown in table 1

2.2. Optimization setup

The optimizations will be divided into different cases to investigate what optimum designs will be found by the optimizer for different power or DDL objectives. This will be done to investigate the effect of different objectives for both upwind and downwind winglets. This work will concern multi-objective optimization, where power will be maximized for and Design Driving Loads (DDLs) will be minimized for. Different DDLs will be minimized in different optimization cases so it can be investigated whether power can be increased without the increase of a DDL.
The optimization technique that will be used to this end is Multi-objective Bayesian Optimization (MOBO). MOBO builds a probabilistic model of the objective function, where the objective function is the aerodynamic performance evaluated by the aerodynamic analysis tool, for which the lifting line code AWSM [11] is used. AWSM's free wake model is used where the wake length is set to three diameters. The simulation time is set to double the time needed for three diameters of wake to convect, so convergence is ensured. The timestep is set to a value that produces angular steps of 10 degrees. Other parameters have been set to their default value as advised by Boorsma et al. [12].
The probabilistic model is called the surrogate model, which is searched by an acquisition function to determine the next design that will be evaluated. A Gaussian Process (GP) is usually used as a surrogate model. This work also investigates the effect of using Bayesian Neural Networks (BNN) as a surrogate model instead of a GP. As the acquisition function, the multi-objective Expected Hypervolume Increase (EHVI) function is used in this work.

2.3. Choice of DDLs

As shown by Loenbaek [1], different DDL constraints result in very different blade designs. Two different DDLs investigated in this work are thrust and root flapwise bending moment, as done by Loenbaek. As this research does not concern aeroelastic optimization, tip deflection is not chosen as DDL. Instead, the flapwise bending moment on another location on the blade is chosen. The location chosen is $\frac{r}{R} = 0.8$ as the influence of the winglet is most apparent on $\frac{r}{R} > 0.8$, although a winglet changes the induced velocities over the whole blade. These three objectives will be minimized for in different optimization runs and will be termed the T, $m_{f,r}$ and $m_{f,0.8}$ cases from here on. Power is maximized for in each optimization case.
Although this work considers multi-objective optimization, only designs which have a lower value for a certain DDL than the baseline DTU 10MW RF design are shown in the results. The results will thus show designs with the highest power and a lower DDL as the 'optimized' design. Other non-dominated design are still investigated whether there is a similarity in winglet parameters for these designs. A non-dominated design is a design for which there is no other design that performs better on all objectives. The non-dominated solutions make up the Pareto front.

3. Lifting line validation

To validate the lifting line code, it is compared against results from CFD generated by Zahle et al [13] for the baseline rotor without a winglet. The C_P and C_T are calculated for different wind speeds in figure 3 and figure 4 respectively. Polars for the FFA-W3 airfoil family has been used which has been 3D corrected by AWSM.

For a wind speed of $8m/s$, a comparison of the normal and tangential loads are shown in figure 5 and 6 respectively. A wind speed of $8m/s$ is chosen as it lies in the constant tip speed ratio range.

4. Results

4.1. Choice of surrogate model

In BO, the surrogate model is responsible for the approximation of the power and DDLs of a parameterized design with given inputs. A requirement of the surrogate model is that its

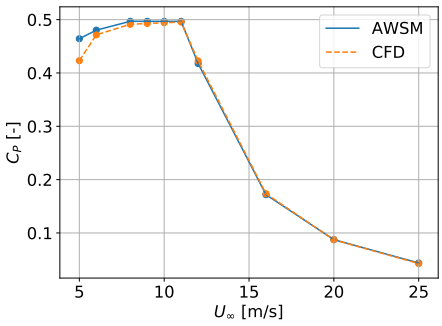

Figure 3. Baseline blade power curve validation for different wind speeds

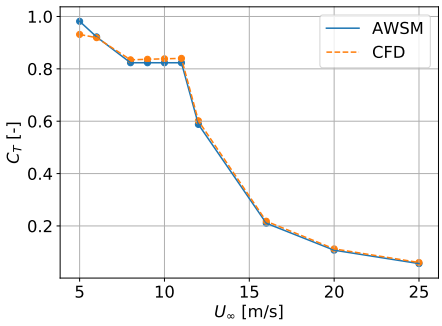

Figure 4. Baseline blade thrust curve validation for different wind speeds

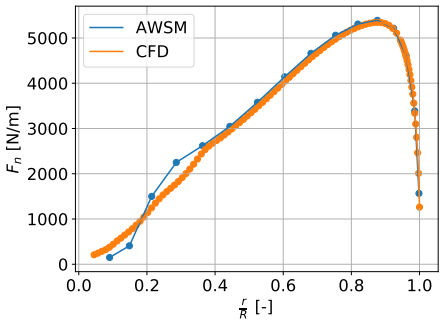

Figure 5. Normal loads validation for $U_\infty = 8m/s$

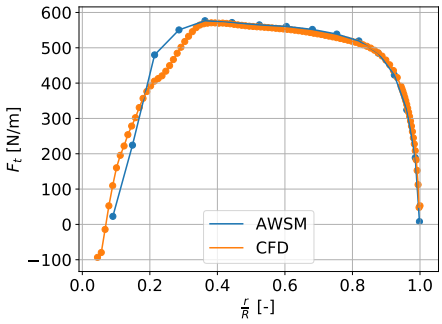

Figure 6. Tangential loads validation for $U_\infty = 8m/s$

prediction is given with an uncertainty estimation, in order for the acquisition function to determine the next design to be evaluated by the lifting line code. The default choice is a GP as the surrogate model for BO. GP will be compared with a BNN, by running the same optimization case twice, once with a GP as the surrogate model, once with a BNN as the surrogate model. A hyperparameter tuning study is done for the GP and BNN. For the GP a Matern 5/2 kernel is used. For a BNN it becomes apparent that two hidden layers performed better on the objectives than one hidden layer. Furthermore, the ADAM optimizer is chosen, batch normalization is applied to the output the layers and a ReLU activation function is chosen. The optimization case chosen is a downwind winglet which is maximized for power and minimized for flapwise bending moment at $\frac{r}{R} = 0.8$. As an indicator for the progress of the optimizer, the hypervolume indicator is used. Usually, in the acquisition function a small number of designs, which is set to ten samples in this work, is generated close to the Pareto front which are then all optimized for EHVI with the predictions of the surrogate function using a gradient optimizer. For the gradient optimizer, the surrogate model is evaluated sequentially until an optimum is found. For a GP these sequential runs can be performed quickly, however, a BNN is slow at performing these sequential runs. A BNN is faster when the samples are presented as batches. Therefore the acquisition function is modified by setting the number of randomly generated samples close to the Pareto front to thousand instead of ten, which are now not optimized for EHVI, but all evaluated quickly by the BNN, after which the candidate design with highest EHVI is chosen. The result for the two optimization runs is shown in figure 7. As seen from the figure, the BNN surrogate model with modified acquisition function is more effective at increasing the

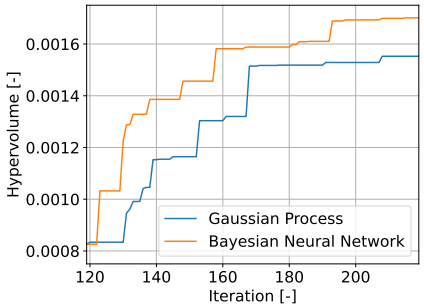

Figure 7. Hypervolume for two optimization runs with different surrogate models

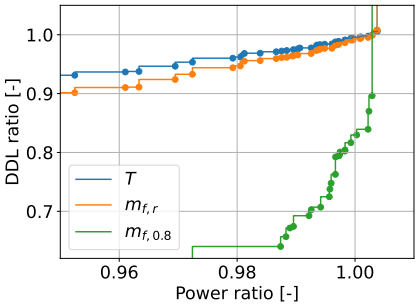

Figure 8. Pareto front for three objectives for the optimization of the blade without winglet

hypervolume and more optimum winglet designs were found using this optimization setup. The BNN will therefore be chosen as the surrogate model for this work. It is expected that the better performance in increasing the hypervolume of the BNN is achieved mostly due to the modification of the acquisition function, since the BNN itself performed worse in estimating the values of the objectives than the GP. More results about the the surrogates models' prediction of the values for objectives can be found in [14]. The combination of a GP and the modified acquisition function would perform much slower, however.

4.2. Optimization of the straight blade

To investigate whether a similar optimum could be achieved without using a winglet, a blade design was optimized for maximum power while minimized for T, $m_{f,r}$ and $m_{f,0.8}$ simultaneously. For this optimization case, the entire blade's chord distribution is optimized. The ratio of the performance between these designs and the baseline DTU 10MW RF blade is plotted in figure 8. As seen from the figure, no high increases in power for the DTU 10MW were found with this optimization setup. The next section will investigate whether an added winglet to the design will result in a higher power increase.

4.3. Optimization of a winglet

A downwind and upwind winglet are maximized for power and minimized for thrust, root flapwise bending moment and flapwise bending moment at $\frac{r}{R} = 0.8$ separately, leading to six optimization cases. All optimizations are run until a stopping criterion has been met. The stopping criterion is set to less than 2% increase in hypervolume for 30 constructive iterations. The blade's chord distribution for $\frac{r}{R} > 0.9$ is also optimized for as the winglet's influence on the loading is most noticeable at this outer part. The Pareto front with actual solutions found shown as a round marker for the optimizations of a downwind winglet are shown in figure 9 and 10 for a downwind and upwind winglet, respectively. The lines in the figures are drawn to illustrate the Pareto front, but mark no actual solutions.

As seen from both figures, multiple designs are found which lead to an increase in power and a decrease in the minimized DDL. For both the downwind and upwind winglet, the Pareto front of the T and $m_{f,r}$ cases are fairly similar in showing high increases in power can be achieved without increasing the T and $m_{f,r}$ above the baseline DTU 10MW RF value. For the $m_{f,0.8}$ case the Pareto front looks different, where lower increases in power can be achieved without increasing the $m_{f,0.8}$ above the baseline DTU 10MW RF value.
To investigate the designs from figures 9 and 10 in more detail, the downwind winglet with the

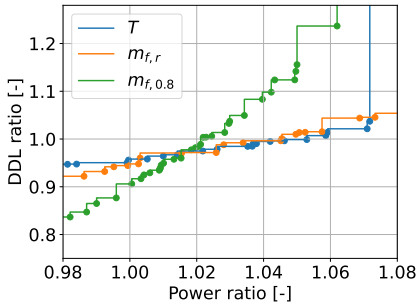

Figure 9. Pareto front for the downwind winglet optimizations

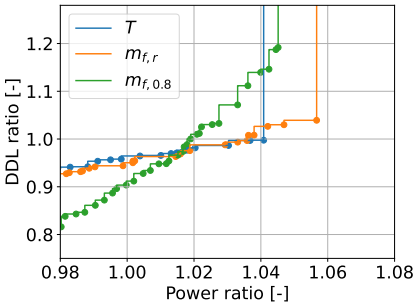

Figure 10. Pareto front for the upwind winglet optimizations

Table 2. Optimized winglets from downwind optimization case

	ΔP [%]	ΔT [%]	$\Delta m_{f,0.8}$ [%]	$\Delta m_{f,r}$ [%]	τ_w [m]	λ [°]	h [m]	ϕ [°]	r_w [m]
T	5.29	-0.12	74.77	0.26	0.40	55.0	7.99	51.56	0.30
$m_{f,r}$	4.51	-0.49	17.53	-0.37	0.22	55.0	7.53	42.31	0.21
$m_{f,0.8}$	2.12	-1.46	-1.12	-0.80	0.22	55.0	8.00	31.10	0.62

highest power not exceeding the DDL of the baseline DTU 10MW RF for each optimization case is shown in table 2, where $\tau_w = \frac{c_{w,t}}{c_{w,r}}$, the taper ratio of the winglet. The chord distribution of the winglets are plotted in figure 11, where the dashed lines indicate the start of the winglet curvature. It can be seen from the table that all three winglets have the maximum allowed

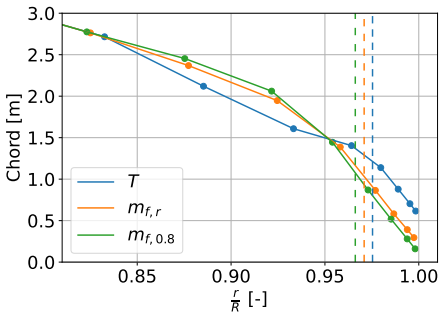

Figure 11. Chord distribution for three optimized downwind winglets

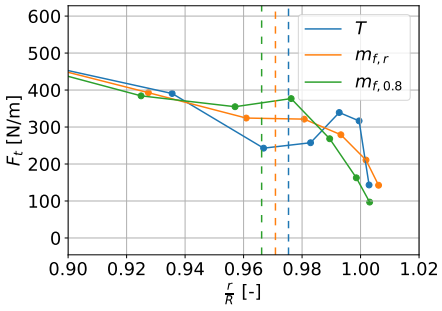

Figure 12. Tangential loads for three optimized downwind winglets

positive sweep, this was found in the majority of all the designs lying on the Pareto front as well. The designs tend to the maximum allowed winglet height as well. All three designs are shown to have a benefit from some cant angle, showing a winglet does perform better than a straight blade for all downwind winglet optimization cases. When minimizing for T or $m_{f,r}$, winglets tend to have a large increase in $m_{f,0.8}$. When minimizing for $m_{f,0.8}$ all winglets with a lower $m_{f,0.8}$ than the baseline DTU 10MW RF value have a lower value for T and $m_{f,r}$ as well. All downwind winglet have positive contribution tangential loads due to a negative induced radial velocity on the winglets. Unswept downwind winglets have a positive induced radial velocity as explained by Gaunaa et al. [2], leading to a negative power contribution of the

Table 3. Optimized winglets from upwind optimization case

	ΔP [%]	ΔT [%]	$\Delta m_{f,0.8}$ [%]	$\Delta m_{f,r}$ [%]	τ_w [m]	λ [°]	h [m]	ϕ [°]	r_w [m]
T	4.08	-0.25	15.30	0.09	0.24	55.0	8.00	0.10	0.10
$m_{f,r}$	3.59	-0.54	18.80	-0.32	0.36	55.0	5.85	5.68	0.10
$m_{f,0.8}$	1.79	-0.97	-1.16	-0.07	0.26	55.0	8.00	0.10	1.06

winglet in the unswept case. The negative induced velocity here, and thus postive tangential loads, is achieved by the positive sweep angle of the winglet, which will be discussed in section 5. The increase in power from the winglet in the $m_{f,r}$ and especially the T optimization case mostly relies on increasing the power on the winglet itself as seen from figure 12. Although not shown in the figure, the winglet from the $m_{f,0.8}$ optimization case mostly achieves an increase in power by increasing the tangential loads on the rest of the blade, while having relatively low loads on the winglet itself. This is achieved by the winglet moving the tip vortex downwind, out of the rotor plane, resulting a less negative axial induced velocity on the blade itself.
The upwind winglets from each case are shown in table 3. The upwind designs' chord distribution and tangential loads is shown in figure 13 and 14 respectively. For the upwind optimization case, the designs again achieved an increase in power from a positive sweep angle, which will also be discussed further in section 5. The upwind designs for all optimization cases, however, did not benefit from a cant angle. Although it was found that a higher cant angle on an upwind winglet does increase the blade's power, it also increases the value for the DDLs. It was found to be more beneficial to keep the blade straight instead of an upwind winglet when considering the trade-off between maximum power and minimum T, $m_{f,r}$ or $m_{f,0.8}$ in all upwind cases.

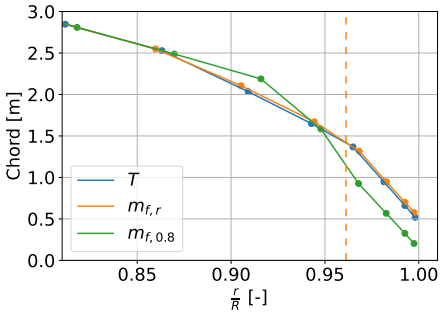

Figure 13. Chord distribution for three optimized upwind winglets

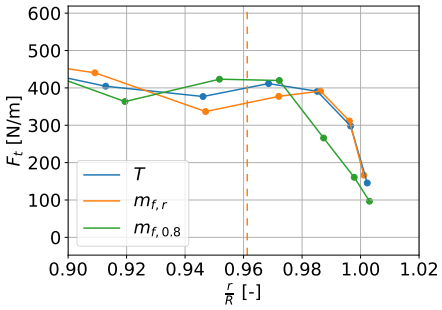

Figure 14. Tangential loads for three optimized upwind winglet

As the power contribution due to the sweep had a high influence on the results, additional optimizations have been done where the winglet sweep was kept constant to a value of zero sweep, although not shown here. From the constant sweep, downwind winglet optimizations similar results were found as for the downwind winglet with variable sweep optimizations, where the winglets from the T or $m_{f,r}$ cases again mostly served to increase the power contribution from the winglet itself and the winglet from the $m_{f,0.8}$ case served to increase the power production of the whole blade. For the upwind winglet optimizations with constant sweep, the same conclusion can be drawn as for the downwind winglet optimization with constant sweep. An upwind winglet did thus have a benefit over a straight blade for the three optimization cases here. The increases in power were slightly lower compared to the downwind cases, however.

4.4. Performance of winglet for other wind speeds

In this work, winglets have been optimized for a single wind speed, which was set to $8m/s$. It was at this wind speed where all objectives were analyzed during optimization without considering another wind speed, and thus the effect the tip speed ratio or pitch would have on these objectives. To gain more insight in how this one-point winglet design perform on other operational conditions, the winglet design is analyzed at the wind speeds for which reference data is available. These wind speeds were shown in figures 3 and 4. The analysis was done with the actual polars instead of dummy polar, after the re-twist of the blade was done. The winglet chosen to analyze at different wind speeds is the winglet design from the optimization case where $m_{f,0.8}$ is minimized, which designs were shown in line three of tables 2 and 3 for the downwind and upwind winglets respectively. The results for the four objectives on different wind speeds is shown in figures 15 and 16. It can be seen that the ratio of every objective is

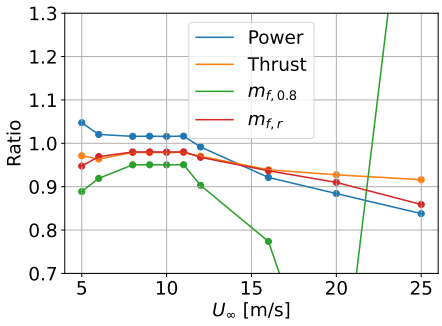

Figure 15. Ratio of the four objectives compared to the baseline blade for the downwind winglet

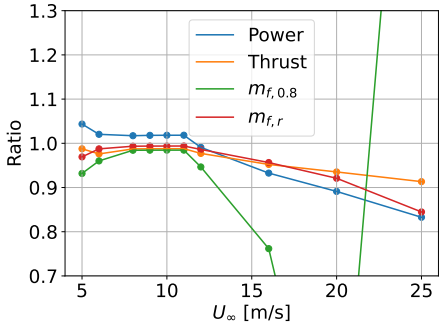

Figure 16. Ratio of the four objectives compared to the baseline blade for the upwind winglet

almost constant for the range of wind speeds with a constant tip speed ratio ($8m/s$ - $11m/s$). Where $7m/s$ is not analyzed here as no validation results were present for this research. It is therefore expected that, were another wind speed chosen in the constant tip speed ratio range, the optimized winglets would have looked the same.

Furthermore, it can be seen that the power ratio is slightly higher for $5m/s$ and $6m/s$ and lower for high wind speeds. This indicates that a winglet is more benificial at lower wind speeds, or high tip speed ratios. However, as was found in the validation section, AWSM was not performing well for these very low wind speeds compared to reference data, as is shown in figure 3 and 3.

The figures have been limited to a ratio of $0.7 - 1.3$ on the y-axis as there was a high increase in the $m_{f,0.8}$ ratio for higher wind speeds. The DTU 10MW RF's maximum flapwise bending moment occurs at $11m/s$, however. The absolute values for $m_{f,0.8}$ are shown in figures 17 and 18 for the downwind and upwind optimized winglet respectively. It can be seen from the figure the maximum absolute $m_{f,0.8}$ does not increase.

5. Discussion

From the optimization runs, it quickly became apparent that the aerodynamic analysis method tended to design winglets with a positive sweep to increase the rotor's aerodynamic power. The sweep gave a high increase in power while other DDLs did not increase by a large amount, as is also found when optimizing a straight unswept and straight swept winglet separately in [14]. This was found for both downwind and upwind winglets, however, the increase in power was larger for a downwind winglet.

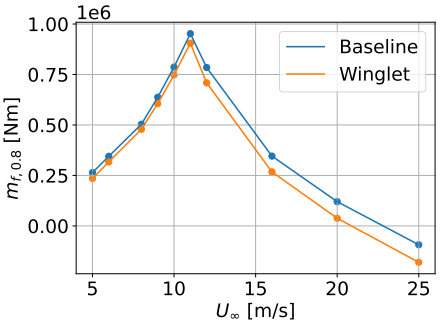

Figure 17. Absolute values of $m_{f,0.8}$ for the optimized downwind winglet

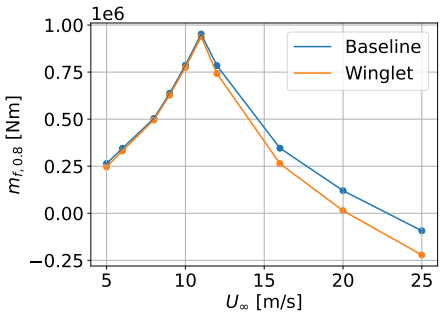

Figure 18. Absolute values of $m_{f,0.8}$ for the optimized upwind winglet

It was found by an external field analysis that downwind in the wake, just downstream of the blade's tip, there is a region with a more negative radial induced velocity, this was found to be true for a blade without a winglet and for a blade with a winglet. Whenever the downwind winglet is swept into this area of reduced induced radial velocity, this would create more tangential loads on the winglet and thus increase the rotor's power. This is shown visually in figure 19, where the freestream is in the positive x-direction and the rotation of the rotor is clockwise from the viewer's perspective. Similarly, for the upwind winglet, just upwind and away from the rotational direction, a zone with increased positive radial induced velocity was found, also leading to increased tangential loads on the winglet, shown in figure 20. Note that the rotation is counter-clockwise from the viewer's perspective here. The significantly

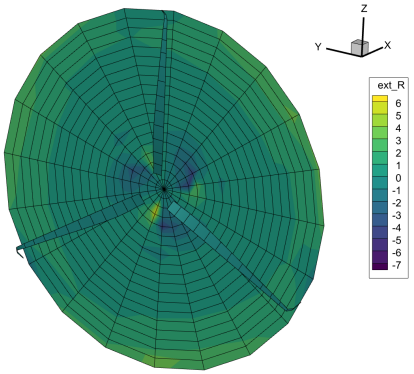

Figure 19. Induced radial velocity (ext_R) field $7.5m$ downwind of a rotor with a swept winglet

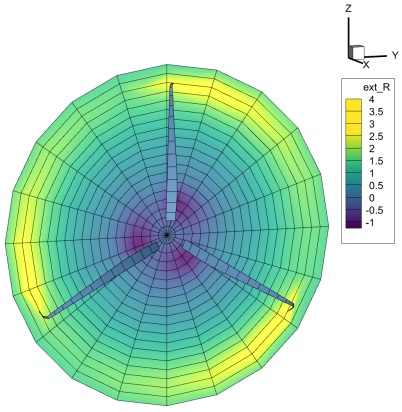

Figure 20. Induced radial velocity (ext_R) field $5m$ upwind of a rotor with a swept winglet

increased performance from the sweep is unexpected, as Munk's stagger theorem [6] states that the induced drag of all wings with the same projected shape and same projected circulation on a plane perpendicular to the freestream is equal. Leading to no increased subsonic aerodynamic performance for sweep in airplane cases. In this work it was found that winglets with the same projected shape did not have the same loads and benefit from a positive sweep angle, contrary to what is true for airplanes. Munk's stagger theorem assumes translatory flow, a planar, drag-free wake and the same circulation distribution. Although the circulation distribution was kept the

same in this sweep analysis using dummy polars, the flow is not translatory and there is no planar wake. This might indicate that without these assumptions being true, sweep can have an aerodynamic benefit to a wind turbine design.
As the lifting line code is not validated against reference data for a case with winglet, this finding would need validation from higher fidelity methods, such as CFD or experimental, for example.
Furthermore, it was found that downwind winglets were still able to increase the power by approximately 2% without exceeding the flapwise bending moment at $\frac{r}{R} = 0.8$. A winglet was more beneficial to the design than a straight tip for a downwind winglet, when constraining the bending moment at $\frac{r}{R} = 0.8$.
When constraining the thrust or root flapwise bending moment, a winglet was also able to increase the rotor's aerodynamic power for a downwind winglet. The winglet designs that were found for these cases mostly increased the power contribution from the winglet itself and barely influenced the power contribution from the blade. This resulted in high flapwise bending moments near the tip.
For optimization cases concerning an upwind winglet, having a zero cant angle, leading to a straight, swept, tip instead of a winglet, let to a more optimal design for all three optimization cases. The increase in power from the designs was due to the positive sweep angle of the tip.

6. Conclusion

Winglet designs have been optimized using the lifting line code AWSM as the aerodynamic analysis method and Bayesian Optimization in combination with a Bayesian Neural Network as optimization framework. The winglets are optimized for one wind speed on the constant tip speed ratio. A few conclusions can be drawn from this optimization study.
Winglet sweep in the downwind direction has shown to significantly increase the power production of a rotor in this work without a high increase in other DDLs. The reason for this increase is believed to be due to regions with more negative and more positive radial induced velocity in the downwind and upwind external velocity field respectively.
When minimizing for the thrust or root flapwise bending moment, winglets that increase the power contribution from the winglet itself are found. These designs led to highly increased flapwise bending moment close to the winglet, however. When minimizing for the flapwise bending moment close to the winglet instead, however, a winglet was still able to increase the power production of the entire blade. The winglet itself had a minimal contribution to the power increase of the design.
Moreover, a modified combination of a surrogate model and acquisition function is proposed for Bayesian Optimization, which achieved more designs lying on the Pareto front than the default choice of a Gaussian Process for this optimization problem.

References

[1] Loenbaek K, Bak C, I Madsen J and Dam B 2020 *Wind Energy Science* **5** 155–170 ISSN 23667451
[2] Gaunaa M and Johansen J 2007 *Journal of Physics: Conference Series* **75** ISSN 17426596
[3] Eppler R 1997 *Aerospace Science and Technology* **1** 3–15 ISSN 12709638
[4] Johansen J and Sørensen N N 2006 *Risø National Laboratory* **1543** 1–17 ISSN 0021-8790
[5] Zahle F, Sørensen N N, McWilliam M K and Barlas A 2018 *Journal of Physics: Conference Series* **1037** ISSN 17426596
[6] Munk M M 1923 *NACA Report 121*
[7] Reddy S R, Dulikravich G S, Sobieczky H and Gonzalez M 2019 *Journal of Solar Energy Engineering, Transactions of the ASME* **141** ISSN 15288986

[8] Briffoteaux G, Gobert M, Ragonnet R, Gmys J, Mezmaz M, Melab N and Tuyttens D 2020 *Swarm and Evolutionary Computation* **57** 100717 ISSN 22106502 URL https://doi.org/10.1016/j.swevo.2020.100717

[9] Stock-Williams C, Chugh T, Rahat A and Yu W 2020 *Machine Learning*

[10] Bak C, Zahle F, Bitsche R, Yde A, Henriksen L C, Natarajan A and Hansen M H 2013 1–138 URL https://dtu-10mw-rwt.vindenergi.dtu.dk

[11] Van Garrel A 2003 *ECN Wind Energy* 106

[12] Boorsma K and Caboni M 2020

[13] Zahle F 2019 DTU 10MW Reference Turbine URL https://rwt.windenergy.dtu.dk/dtu10mw/dtu-10mw-rwt/

[14] Leenders N 2021 Vortex-model-based Multi-objective Optimization of Winglets for Wind Turbines using Machine Learning Tech. rep. Delft University of Technology